The 27th Meeting on Image Recognition and Understanding

Quantification of Overlapped Fluorescent Dyes via Autoencoder with Simultaneous Optimization of LCVR Voltage Selector and Quantifier

Kazuma Fujiwara[1,a)] Takuya Funatomi[1] Kazuya Kitano[1]
Yuki Fujimura[1] Yasuhiro Mukaigawa[1] Hiroshi Ochiai[2]

Abstract

Conventional fluorescence microscopy avoids the use of fluorescent dyes with overlapping emission spectra to prevent crosstalk, limiting the variety of usable dyes and increasing experimental time for complex samples, such as those with extensive RNAs. We propose a novel method for direct quantification of fluorescent dye concentrations from a limited number of images, bypassing the need to restore the spectral distribution, typically an ill-posed problem. This is achieved by modulating light with a Liquid Crystal Variable Retarder (LCVR) and modeling the LCVR within an autoencoder framework using physics-based 2D Multilayer Perceptron (MLP) regression. Our approach innovatively optimizes the LCVR voltage selector (encoder) and concentration quantifier (decoder) simultaneously. The effectiveness of our proposed methodology has been demonstrated through both simulation experiments and measurements, confirming its practical application.

1. Introduction

RNA sequencing (RNA-seq) has revolutionized biology by enabling gene expression analysis across whole tissues and cell populations. Spatial transcriptomics, an emerging technique, maps gene expression while retaining spatial information within tissues, offering insights beyond conventional RNA-seq. This method enhances our understanding of cellular functions in vivo, with implications for developmental biology and drug discovery. Traditional approaches, such as seqFISH [3], detect numerous RNA species through repeated hybridization and fluorescence detection cycles using fluorescent-labeled DNA probes. The method can detect up to 24,000 different RNA molecular species. However, the procedure requires a total of 80 rounds of hybridization and image acquisition, with each round taking approximately an hour. Notably, after every set of ten hybridizations, manual experimental manipulations are necessary. Therefore, this repetitive process is time-consuming and labor-intensive.

If many fluorescent dyes can be used simultaneously, the number of hybridizations and reprobing can be reduced, thereby improving the efficiency of the analysis. However, due to the limitation of overlapping fluorescence spectra, general fluorescence microscopes can use only a few types of fluorescent dyes at most.

The objective of this study is to develop a method that can stably detect multiple fluorescent dyes without being affected by the overlapping spectra of fluorescent dyes. This is expected to enable high-throughput seqFISH analysis with fewer rounds, facilitating spatial transcriptomics and leading to speed and cost reduction. As a result, the whole research field based on genome analysis will be further stimulated.

2. Related work

Fluorescence detection methods. While fluorescence microscopy struggles to detect multiple fluorescent dyes due to spectral overlap, hyperspectral imaging offers a solution by constructing spectral cubes. However, this approach's higher spectral resolution compromises signal strength and lowers the signal-to-noise ratio, posing challenges for detecting weak signals [4], [6], [7].

Spectral Imaging with Liquid Crystal Variable Retarder (LCVR). Alternative approaches include coded sensing for indirect measurement, enhancing sensitivity. LCVR combined with polarizers can maintain higher fluorescence intensity, reducing noise effects. August *et al.* [1] and Yang *et al.* [8] demonstrated hyperspectral imaging with LCVR, achieving high spectral resolution through dozens to hundreds of observations. While these methods enable the quantification of dyes with overlapping spectra, the reconstruction of extensive spectral channels is often more than needed for practical dye quantification.

Quantification of Fluorescent Dyes Concentration via Sparse Modeling. Direct quantification of fluorescent dyes without reconstructing the spectral distribution allows for the avoidance of ill-posed problems since the dimension of the concentration vector is significantly smaller than the wavelength resolution of the spectral distribution. We employed an LCVR as a spectral modulator to construct a dye dictionary and utilized LASSO-LARS for quantifying

[1] Nara Institute of Science and Technology
[2] Kyushu University
[a)] fujiwara.kazuma.fj4@is.naist.jp

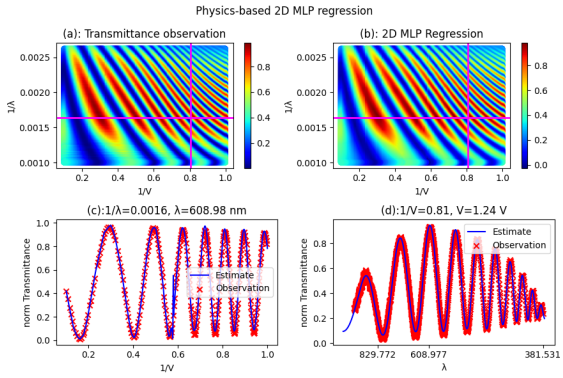

Fig. 1 The spectral transmittance of the spectral modulator and the result of MLP regression.

their concentrations [5]. This method has been validated through simulation experiments; however, actual device validation has not been performed, and optimization of the voltage selection for the LCVR has not been conducted. Thus, this study demonstrates the concept of directly quantifying fluorescent dye concentrations without spectral distribution reconstruction using a simplified implementation of the decoder.

3. Method

Building upon the concept of fluorescence detection without spectral cube reconstruction using a spectral modulator from our prior study [5], we employ an Multilayer Perceptron (MLP) for "*Concentration Quantification*", which acts as the decoder in an Autoencoder framework, where the encoder serves dual roles, functioning as an "*LCVR Voltage Selector*" in addition to the spectral modulator in the imaging process. By training this Autoencoder, we can simultaneously achieve voltage settings optimization and efficient quantification of fluorescent dye concentration.

3.1 Spectral coding

The spectral modulator consists of an LCVR and two polarizers. The LCVR is oriented at 45° to the axis of the polarizers. The spectral transmittance can be modulated according to the voltage applied to the LCVR as

$$t(\lambda, V_k) \propto \frac{1}{2} - \frac{1}{2}\cos\left(\frac{\Delta n(V_k,\lambda)d}{\lambda}\right), \qquad (1)$$

where λ is the wavelength, d is the thickness of LCVR, $\Delta n(V_k,\lambda)d$ is the birefringence at LCVR voltage V_k and λ [9]. Also, $\frac{\Delta n(V_k,\lambda)d}{\lambda}$ is the amount of phase difference of LCVR and is called retardance. Figure 1(a) show the spectral transmittance of the spectral modulator.

When a spectral modulator is placed in front of the sensor, the spectral distribution incident on the image sensor becomes the multiplication of the spectral distribution of the fluorescent-labeled targets, the spectral sensitivity characteristics of the sensor, and the spectral transmittance of the spectral modulator. Then, the intensity observed by the sensor is obtained by integrating it over the observable range. The spectral distribution of the fluorescent targets

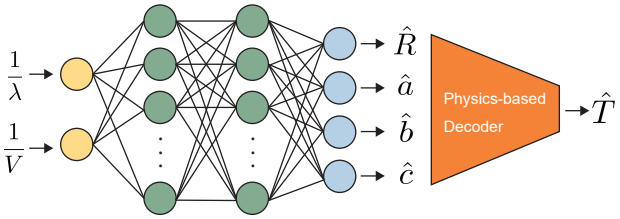

Fig. 2 Encoder module of spectral encoder.

can be expressed as a sum of individual dye contributions [2]. The intensity at a given voltage V_k is described by

$$i_k = \sum_{j=1}^{P} c_j \int r_j(\lambda) t(\lambda, V_k) s(\lambda) d\lambda, \qquad (2)$$

where $s(\lambda)$ is the spectral sensitivity of the sensor, P is the number of different fluorescent dyes present in the whole sample, c_j and $r_j(\lambda)$ represents the concentration and the emission spectrum of the j-th fluorescent dye, respectively.

This intensity i_k varies with voltage, and by changing the voltage N times, we can obtain an N-dimensional spectral code that is unique to the input spectral distribution. The N-dimensional spectral code is described by

$$\mathbf{i} = \begin{bmatrix} i_1 & \cdots & i_k & \cdots & i_N \end{bmatrix}^\top. \qquad (3)$$

3.2 Modeling the Spectral Modulator through Physics-Based 2D MLP Regression

In our approach, the spectral modulator functions as the encoder within the autoencoder framework. For effective optimization, it's crucial that this component be differentiable. Given the disparity between the ideal mathematical models and the actual behavior of spectral modulators, as illustrated by Eq. (1), the development of a continuous and differentiable surrogate model is imperative. Therefore, we have adjusted Eq. (1) to introduce a model that better aligns with real-world behavior, as detailed below:

$$t\left(\frac{1}{\lambda},\frac{1}{V}\right) = a\left(\frac{1}{\lambda},\frac{1}{V}\right)\cos\left(R\left(\frac{1}{\lambda},\frac{1}{V}\right) + b\left(\frac{1}{\lambda},\frac{1}{V}\right)\right) + c\left(\frac{1}{\lambda},\frac{1}{V}\right) \qquad (4)$$

where R represents the retardance. The ability to set each variable non-linearly offers high expressiveness, making it adequate for modeling the spectral modulator.

For capturing the complex spectral transmittance characteristics of the spectral modulator, we adopt a physics-based 2D MLP regression (Fig. 2) that consists of fully connected layers and uses $1/\lambda$ and $1/V$ corresponding to the transmittance t_{obs} measured by a spectrometer as inputs. It outputs the estimated variables $\hat{R}$, $\hat{a}$, $\hat{b}$, and $\hat{c}$. These estimates allow for the calculation of the estimated transmittance $\hat{T}$ using Eq. (4), effectively functioning as a physics-based decoder. Figure 1(b) show a result of MLP regression.

Using the encoder module, we synthesize concentrations drawn from a prior distribution and corresponding spectral codes (Eq. (3)) for training autoencoder. Subsequently, we

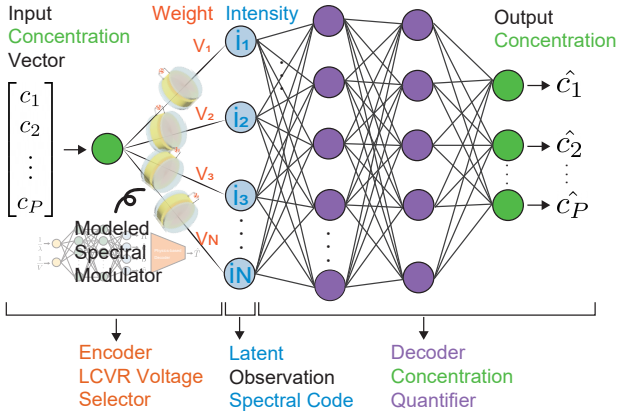

Fig. 3 Network overview of the autoencoder.

train a decoder that outputs concentration from the spectral code. Unlike a simple model that generates spectral codes from given voltages, the encoder model takes a voltage as input and optimizes it as a trainable parameter via back-propagation.

3.3 Autoencoder with Simultaneous Optimization of LCVR Voltage Selector and Quantifier

Under the constraints of a given number of observations N and a specific set of dyes (total number P), a set of N encoder modulators allow it to function as an LCVR Voltage Selector selecting the optimal set of voltages. Thus, unlike simple autoencoders that only utilize a decoder, our approach enables the simultaneous optimization of both the LCVR Voltage Selector and Concentration Quantifier, as illustrated in Fig. 3. The encoder must faithfully replicate the spectral coding process described in Section 3.1. Utilizing the spectral transmittance model of the spectral modulator shown in Fig. 2, we designed the encoder as a custom layer that generates spectral codes corresponding to a specific set of fluorophores based on Eq. (2) and Eq. (3).

The decoder is designed using an MLP with fully connected layers. By extracting only the decoder part from the autoencoder, we can construct a network that takes spectral codes as input and outputs the concentration of fluorescent dyes. This enables the decoder to function as a Concentration Quantifier. Our autoencoder employs a conventional loss function defined as:

$$\text{Loss} = \text{MSE}(\mathbf{c} - \hat{\mathbf{c}}), \tag{5}$$

where $\hat{\mathbf{c}} = \begin{bmatrix} \hat{c_1} & \hat{c_2} & \cdots & \hat{c_P} \end{bmatrix}^\top$ represents the estimated concentration vector.

Through training with this loss function, our autoencoder achieves the simultaneous optimization of the LCVR Voltage Selector (Encoder) and Concentration Quantifier (Decoder), distinguishing our method from existing techniques. This approach allows for the accurate quantification of fluorescent dye concentrations while efficiently utilizing the complex characteristics of the spectral modulator.

dye	ground truth	our method	PSNR (dB)
ATTO 490			54.95
Alexa 488			55.97
ATTO 565			48.54
Alexa 594			58.14
Alexa 647			55.03
Alexa 700			55.43
Alexa 750			51.72

Fig. 4 Quantification results of simulation experiment.

4. Experiments

4.1 Spectral modulator modeling using 2D MLP regressor

To implement the spectral modulator modeling in actual devices through physics-based 2D MLP regression, we built a spectral modulator and measured its spectral transmittance. We employed Thorlabs LCC1115-A as an LCVR and Thorlabs WP25M-VIS visible wire grid polarizer for the polarizers. We measured the transmittance using an Ocean Optics Maya2000 Pro spectrometer. By consulting the retardance data of LCC1115-A at 633 nm and 25 °C provided by Thorlabs, we selected 331 voltage values V_k to ensure constant retardance changes within the voltage resolution of the function generator (Rigol DG4162), expecting to achieve more varied spectral transmittances. This approach yielded real-world measurements of spectral transmittance, t_{obs}, corresponding to λ and V_k. The outcomes of the 2D MLP regression can be visually examined in Fig. 1.

4.2 Principle Verification through Simulation

A simulation based on seqFISH fluorescence images was performed to verify the quantification principle. We prepared seven distinct fluorescence images representing various RNA molecule species as the ground truth. To add realism to our simulation and introduce a prior distribution of concentrations, an additional set of RNA distributions was prepared and randomized before inclusion in our training dataset. After setting up normalized fluorescence spectral distributions and a selection of ten voltages within the learning dataset for the autoencoder depicted in Fig. 3, the LCVR Voltage Selector identified an optimal set of ten voltages, and the Concentration Quantifier was trained accordingly. By applying the Concentration Quantifier to quantify fluorescence using the spectral code derived at these optimized voltages, the results displayed in Fig. 4 were obtained.

These results demonstrate the capability of our method to quantitatively determine concentrations with high accuracy, indicated by PSNR values over 45, for seven dyes using a reasonable number of voltage selections. This highlights the feasibility of our approach under ideal conditions.

4.3 Experiment using real setup

Experimental setup. We built an experimental setup

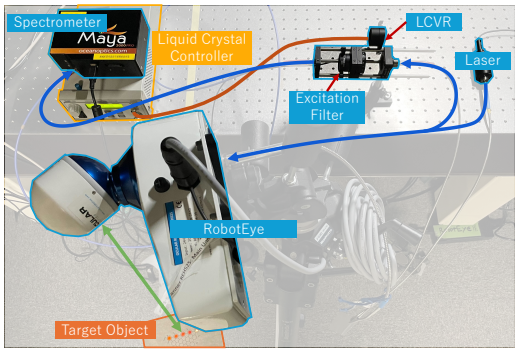

Fig. 5 Experimental setup.

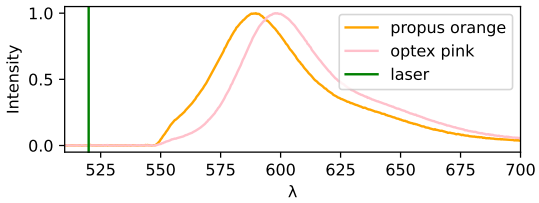

Fig. 6 Spectral distribution of ink from fluorescent pens.

as shown in Fig. 5. Though monochrome camera would suffice for imaging, we constructed a system capable of detailed hyperspectral imaging for obtaining a reference data. We employed RobotEye REHS25 scanner (Ocular Robotics Ltd), a Maya2000 Pro spectrometer (Ocean Optics, Inc.), a bifurcated optical fiber, LCC25 LCVR voltage controller (Thorlabs). We input 520nm laser light as excitation into one fiber and collect reflected light containing fluorescence from the other fiber. Additionally, a detachable spectral modulator and an excitation filter were placed between the spectrometer and scanner to cut the laser light.

Measurement Targets. Instead of RNA, ink from fluorescent pens was used as the target in our experiments. Specifically, orange fluorescent pen ink (Mitsubishi Pencil PUSR-80.4, referred to as *Orange*) and pink fluorescent pen ink (ZEBRA RWK8-P, referred to as *Pink*) were used as shown in Fig. 6. We attempted to separate two types of fluorescent dyes that could be linearly separated through spectral measurement, establishing a baseline and comparing it with estimated results. Standard solutions of the original inks were used to create three mixtures of the dyes in ratios (Orange, Pink) = (30, 10), (20, 20), (10, 30) [µL]. The original inks of Orange and Pink, as well as their mixtures, were applied to Japanese paper.

Experimental Method. Using the constructed setup, we measured the fluorescent spectrum of the targets. Spectral measurements were taken with the spectral modulator inserted to acquire $r_j(\lambda)t(\lambda, V_k)s(\lambda)$, and without the modulator to obtain $r_j(\lambda)s(\lambda)$. The voltage input to the spectral modulator was determined by training the autoencoder depicted in Fig. 3 with the same dataset as in Section 4.2, setting the spectral distribution of the normalized inks and the number of voltage selections to ten. Different from the simulation experiment, we measured the spectral transmittance of the spectral modulator at the optimized voltages to fill the gap between simulation and real setup, and retrained the Concentration Quantifier accordingly.

	Amount [µL]		Estimated $\tilde{c_j}$ [%]		x	Residual
	Orange	Pink	Orange	Pink		
(a)	30	10	60.9	39.1	1.78	8.5
	20	20	49.2	50.8		6.0
	10	30	28.4	71.6		4.8
(b)	30	10	54.4	45.6	2.21	2.7
	20	20	36.3	63.7		5.5
	10	30	8.2	91.8		4.7

Table 1 Quantitative results of fluorescent quantification by (a) our method and (b) baseline from spectra.

Evaluation. While the molar concentration of RNA dyes is known, it is not for the inks of the fluorescent pens. Therefore, even when mixing different concentrations of fluorescent inks at known ratios, the ratios do not correspond to c_j. However, the molar concentration of the standard solution should be consistent across different mixtures, and this consistency was used for evaluation. Specifically, the ratio of c_j estimated from the three types of mixtures ($\tilde{c_j}$) was used to estimate the molar concentration ratio x between Orange and Pink, and the residual was calculated for quantitative evaluation.

Experimental Results and discussion. The fluorescent intensity $\mathbf{i}$ of the measurement targets was calculated by summing the spectral distribution obtained through the spectral modulator at ten selected voltages determined by the Voltage Selector. The learned Concentration Quantifier was then used to estimate the concentrations of Orange and Pink. The estimated concentration ratios $\tilde{c_j}$ for each mixture are shown in Table 1(a). For comparison, $\tilde{c_j}$ estimated using spectral distributions measured without the spectral modulator are shown in (b). The molar concentration ratio x estimated from the three mixtures' $\tilde{c_j}$ and the residual between the estimated and reconstructed ratios of c_j are also presented. Although the true molar concentration ratio is unknown, the residuals indicate that our method, despite a slight degradation, was able to estimate ratios from a limited amount of data compared to the traditional method.

5. Conclusion

This study presents a novel method for directly quantifying fluorescent dyes with overlapping spectra using a LCVR within an autoencoder framework. Our approach successfully optimizes LCVR Voltage Selector and Concentration Quantificator simultaneously. Through simulations and real-world experiments, we've demonstrated the method's feasibility. Future work will aim to further refine the optimization process, including optimizing the number of voltage selections and the set of dyes, promising more efficient and broad applications in biological research and related fields.

Acknowledgement This work was partly supported by JST PRESTO JPMJPR2025 and JST CREST JPMJCR23N3.

References

[1] August, I., Oiknine, Y., AbuLeil, M., Abdulhalim, I. and Stern, A.: Miniature Compressive Ultra-spectral Imaging System Utilizing a Single Liquid Crystal Phase Retarder, *Scientific Reports*, Vol. 6, No. 1 (2016).

[2] Dickinson, M., Bearman, G., Tille, S., Lansford, R. and Fraser, S.: Multi-Spectral Imaging and Linear Unmixing Add a Whole New Dimension to Laser Scanning Fluorescence Microscopy, *BioTechniques*, Vol. 31, No. 6, pp. 1272–1278 (2001).

[3] Eng, C.-H. L., Lawson, M., Zhu, Q., Dries, R., Koulena, N., Takei, Y., Yun, J., Cronin, C., Karp, C., Yuan, G.-C. and Cai, L.: Transcriptome-scale super-resolved imaging in tissues by RNA seqFISH+, *Nature*, Vol. 568, No. 7751, p. 235–239 (2019).

[4] Hagen, N. A. and Kudenov, M. W.: Review of snapshot spectral imaging technologies, *Optical Engineering*, Vol. 52, No. 9, p. 090901 (2013).

[5] Kazuma Fujiwara, Takuya Funatomi, K. K. Y. F. Y. M. H. O.: Detection of Multiple Fluorescent Dyes Using Liquid Crystal Variable Retarder and Sparse Modeling, *Electronic Imaging*, pp. 161–1 – 161–5 (2024).

[6] Li, Q., He, X., Wang, Y., Liu, H., Xu, D. and Guo, F.: Review of spectral imaging technology in biomedical engineering: achievements and challenges, *Journal of Biomedical Optics*, Vol. 18, No. 10, p. 100901 (2013).

[7] Renkoski, T. E., Utzinger, U. and M.D., K. D. H.: Wide-field spectral imaging of human ovary autofluorescence and oncologic diagnosis via previously collected probe data, *Journal of Biomedical Optics*, Vol. 17, No. 3, p. 036003 (2012).

[8] Yang, T., Xu, Z., Ren, W., Feng, Y., Wu, D., Zhang, R. and Xie, Y.: Compressive hyperspectral microscopic imaging using spectral-coded illumination, *Optics & Laser Technology*, Vol. 166, p. 109631 (2023).

[9] Yariv, A. and Yeh, P.: *Optical waves in crystals*, Pure & Applied Optics S., John Wiley & Sons, Nashville, TN (1984).